Journal of Archaeological Science 35 (2008) 2614–2623

Contents lists available at ScienceDirect

Journal of Archaeological Science

journal homepage: http://www.elsevier.com/locate/jas

Integrated seismic tomography and ground-penetrating radar (GPR) for the high-resolution study of burial mounds (*tumuli*)

E. Forte, M. Pipan*

Università di Trieste, Department Geological, Environmental and Marine Sciences (DISGAM), via Weiss 1, 34127 Trieste, Italy

ARTICLE INFO

Article history:
Received 27 December 2007
Received in revised form 14 April 2008
Accepted 28 April 2008

Keywords:
Geophysics
Archaeology
Seismic tomography
Ground-penetrating radar
Burial mound
Tumulus
3-D interpretation

ABSTRACT

The study primarily aims at providing adequate imaging resolution of large and prominent targets of archaeological interest, such as pyramids and *tumuli*, at all depth levels. We implemented an integrated seismic tomography and georadar (STG) technique to perform high-resolution imaging and characterization of *tumuli* (burial mounds). We tested the proposed technique on a preserved late Bronze Age burial mound in northern Italy, for which STG succeeded in performing an accurate 3-D reconstruction of the structure and stratigraphy as proved by later archaeological excavations. We completed two transmission seismic tomography measurements, at present ground level and at 1.5 m elevation, with a 24-channel seismograph and 15° angular separation between geophones. The ground-penetrating radar (GPR) dataset encompasses 12 250 MHz radial profiles and 12 common mid point gathers for velocity analysis. Shallow layers of the mound are successfully imaged by GPR, whilst the structure of the deep central part of the tomb is reconstructed from seismic traveltime inversion. In particular, GPR images lenses and layers of sediments forming the external part of the *tumulus*, evidences of a looting attempt, peripheral structures associated with later exploitation of the mound (furnaces) and, in the external sector of the tumulus, the top of the deep layer of silty sediments covering the funeral chamber. Tomographic results reveal seismic velocity anomalies of potential archaeological interest at ground level, which were successively validated by archaeological excavations. The integration of GPR and tomographic datasets is an effective strategy to overcome the imaging and interpretation problems related to the structure of such peculiar funeral monuments. STG can be applied to a virtually unlimited dimensional range and requires a limited data acquisition, processing and inversion effort. The results of the study allowed the identification of the funeral chamber and a detailed imaging of layering and structural details.

© 2008 Elsevier Ltd. All rights reserved.

1. Introduction

Pyramids and *tumuli* (burial mounds) are challenging targets for archaeological exploration because their architectural significance is comparable with the archaeological importance of their content and traditional methods (archaeological excavation) allow access to the content only by dismantling the structure itself.

Tumuli with individual or collective funeral chambers have worldwide distribution starting at the beginning of the Neolithic period (Hodder, 1984) and represent characteristic burial architecture of several cultures. *Tumulus*-like structures are also known as barrows, cairns or *kourgans* depending from geographical location, their shape and cultural origin. Preserved burial mounds are found along the Silk Route, in mountain ranges of Central Asia, in central and northern Europe, Japan, Africa and America and in several regions of the Mediterranean area. They are made of different materials ranging from large boulders to silty or clayed soils, wood and adobe. From the archaeological point of view, burial mounds offer opportunities to gain insight into burial architecture and to reconstruct important information about life and customs during the building period (see e.g. Renfrew and Bahn, 2000). From the geophysical point of view, burial mounds are challenging targets, which encourage implementing non-conventional techniques to attain the level of subsurface penetration and resolution required to study internal structure and to better plan archaeological excavations.

Geophysics provides effective solutions for their non-invasive exploration (see e.g. Tsokas et al., 1995 and Pipan et al., 2001) and can therefore offer important information to the archaeological teams for the preliminary study of the structure and to plan the excavation. From the geophysical point of view, pyramids and *tumuli* allow access from all sides but the base, which means that sensors and sources can be deployed in 3-D geometries to surround the target. Such peculiarity allows combinations of data acquisition

* Corresponding author. Tel.: +39 040 558 2277; fax: +39 040 558 2290.
E-mail address: pipan@units.it (M. Pipan).

0305-4403/$ – see front matter © 2008 Elsevier Ltd. All rights reserved.
doi:10.1016/j.jas.2008.04.024

techniques that require boreholes and surface experiments in geophysical common practice.

In this work we focus on the geophysical study of *tumuli* with the primary objective of obtaining the maximum possible resolution at all depths of archaeological interest. On such purpose, we exploit a combination of electromagnetic [ground-penetrating radar (GPR)], and seismic techniques.

The proposed integrated seismic tomography and georadar (STG) technique accomplished both tasks through a 3-D reconstruction of subsurface structure and allowed to locate the funeral chamber and the sectors excavated by looters.

1.1. Previous geophysical studies

Geophysical studies of *tumuli* and mound-shaped objects are reported in literature and are based on different approaches. Several authors extensively applied electromagnetic induction techniques (Bevan, 1983; Dalan, 1991; Fröhlich Gugler and Gex, 1996) with the primary objective of measuring variations of conductivity. Such methods allow relatively rapid investigations of large areas but the resolution level is rather low. Moreover, background conductivity can be considered a function of topography, but is calculated from empirical relations, which are valid in specific conditions (Monier-Williams et al., 1990).

Magnetic methods can provide excellent results and can be used during different excavation steps (Morariu et al., 1989; von der Osten-Woldenburg et al., 2002; Becker and Fassbinder, 2001), but they fail to provide 3-D subsurface images and they are most effective where shallow targets contain quantities of ferrous materials or ferrimagnetic minerals, such as maghemite and magnetite. Presence of maghemite is mainly due to natural or man-made fires (Le Borgne, 1960) while fossils of magnetic soil bacteria influence the content of *in situ* formed magnetite (Fassbinder et al., 1990). The most successful examples of application of the method basically come from mapping shallow targets with strong magnetic contrast in low noise conditions.

Further integrated methods, such as the combined application of slingram, gradiometer and ground-penetrating radar are proposed by Persson and Olofsson (2004).

Seismic techniques were also tested to locate funeral chambers and other man-made features buried in mounds. Different strategies are reported such as seismic refraction (Tsokas et al., 1995), crosshole seismic tomography (Louis, 2001) and transmission seismic tomography (Xu and Stewart, 2002; Polymenakos et al., 2004).

Refraction and crosshole techniques seem applicable only in favorable conditions (presence of large buried ramps, wide cavities) and provide information about limited parts of the structures. The most robust and promising approach for funeral chamber detection is probably transmission seismic tomography. Shape and dimensions of the *tumulus* do not affect the applicability of such technique, which can be adapted to site and target characteristics. A sledgehammer can provide adequate energy in most, if not all, cases of archaeological interest and the results of tomographic surveys can be enhanced by reducing the angular interval between sensors around the mound.

Ground-penetrating radar (GPR) is being extensively used in archaeological prospection for pre-excavation and non-destructive studies (Brooke and Maillol, 2007; Whiting et al., 2001; Pérez Gracia et al., 2000). In this work we integrate seismic tomography with GPR to increase resolution at all depth levels and specifically in the peripheral sectors, where limited angular coverage results in poor tomographic results.

2. Methods

The schematic structure of a *tumulus* (Fig. 1) encompasses a burial chamber, at or below ground level, usually covered by cobbles/boulders and by layers of fine grained sediments often alternated with layers of stones of variable dimensions. The funeral chamber may be in central position but is more often eccentric and it is normally enclosed with wooden or stone walls and roof. The 3-D shape of *tumuli* may vary from approximately conical to that of a capsized cup, characterized by dip of the flanks increasing with distance from the center of the mound. The dimensions may vary from few a (4–5) meters in diameter and less than 1 m of maximum elevation to more than 100 m of diameter and 15–20 m of elevation. Some *tumuli* enclose more than one funeral chamber with ramps or other additional inner structures.

Archaeological excavation of *tumuli* is a costly, time-consuming and very invasive task, because it requires removal of large quantities of material and classification and mapping of each removed layer before reaching the burial chamber level. Burial chambers are frequently displaced from central position, to make looting attempts more difficult. Therefore archaeologists normally dig exploratory trenches to identify the location of the chamber and successively focus their efforts on the sectors of major interest.

Geophysical exploration can help in the reconstruction of the inner structure and in locating the funeral chamber, but limitations often occur that are related to dimensions, building materials and type of targets. *Tumuli* can reach up to 20 m in elevation and 100 m in diameter, their morphology is normally quite regular, in the absence of looting attempts or successive use for other purposes, and they are characterized by heterogeneous materials (from boulders to clay) normally laid in lenses and layers of irregular thickness and geometry. Primary objectives in the study of *tumuli* are the localization of the burial chamber and the detailed study of stratigraphy and of further subsurface structures, such as ramps, chambers, tunnels/shafts related to the original constructions or to successive looting attempts.

A combination of seismic tomography and ground-penetrating radar (STG) allows to study *tumuli* and, in general, mound-shaped structures in a virtually unlimited range of dimensions. A large topographic gradient normally is the main geometric characteristic of *tumuli* and sets the basic constraints for seismic and GPR surveys. In particular, rapid changes in elevation require increased

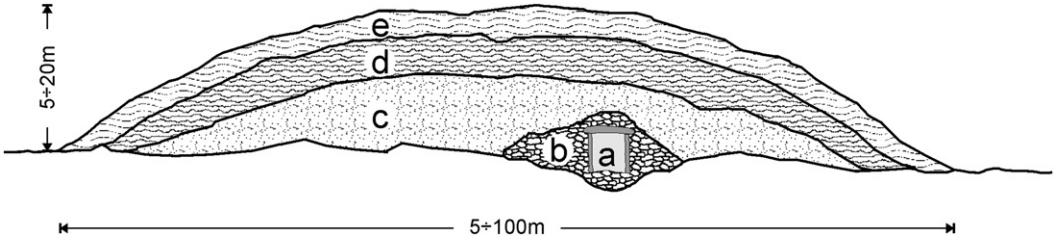

Fig. 1. Schematic structure of a *tumulus*: (a) burial chamber; (b) deep cover made of cobbles and boulders, occasionally of wood; (c) silty and clay rich sealing sediments; (d) alternated layers and lenses of sediments with different grain size; (e) surface cover.

processing effort for seismic and GPR reflection surveys, because accurate static corrections or topographic migration are required (Cox, 1999; Lehmann and Green, 2000).

2.1. Seismic tomography

Tomographic inversion can exploit direct, refracted, reflected or diffracted events and aims at reconstructing the kinematic and/or dynamic characteristics of a medium through a detailed mapping of velocity and/or attenuation. Such operation is based on the measurement of traveltimes and/or amplitudes obtained from a set of source-receiver pairs. Any source-receiver geometry can in principle be exploited, if seismic rays provide complete angular coverage of each subsurface point. In a 2-D case, each point of the study slice should be crossed by seismic waves coming from a 2π angular range with dense angular sampling. In the general case, deployment of sensors and sources on a flat topographic surface constrains the angular coverage attainable and requires picking and numerical simulation of reflected, refracted and diffracted events. In the specific case of mound-shaped structures, 2-D seismic tomography at constant elevation planes allows optimum angular coverage and minimum data acquisition/inversion effort, because a simple transmission scheme can be implemented. The only constraint in data acquisition geometry is to keep constant the elevation of sources and geophones. Angular sampling interval and number and spacing of the selected elevation levels affect the resolution attainable. By adding sources and receivers around the mound at small angular interval we obtain information from most of the model function's cells, while closely spaced elevation levels allow more detailed tracking of traveltime/attenuation variations as a function of depth (see e.g. Tien-when and Inderwiesen, 1994).

Tomographic inversion starts from traveltime/amplitude picking for traces all source-receivers pairs and is based on an initial velocity/attenuation model. Data analysis and previous stratigraphic and geological information, if available, typically drive the initial model definition. The model is then updated after comparison of the observed traveltime with those calculated from the model (see e.g. Tien-when and Inderwiesen, 1994).

A traditional way for solving the inverse problem is to divide the region between source and receiver positions into cells and to find perturbations of the initial model that minimize the differences among calculated and observed traveltimes/amplitudes. The perturbation is assumed to be constant within each cell. The final result of the tomographic inversion is the initial model corrected by the set of optimum perturbations. The traveltime t_i of the generic ith ray is given by:

$$t_i = \sum_{j=1}^{N} A_{ij} s_j$$

where A_{ij} is the distance traveled across the jth cell by the ith ray, s is the slowness of the jth cell and N is the total number of cells (pixels, in a 2-D case). Obviously A_{ij} is null if the ith ray does not cross the jth pixel. We obtain an overdetermined system of equations by defining the traveltime as a column vector t, the slowness as a column vector s, and A the matrix of the raypath intercepts:

$$As = t$$

The system of equations must be solved for the slowness vector s, obtaining in this way the seismic velocity of each cell. The same approach can be used considering both velocity and attenuation. Since matrix s is typically very large, formal matrix inversion is not feasible (Worthington, 1984).

2.2. GPR

Ground-penetrating radar (GPR) is a pulsed electromagnetic technique designed to detect dielectric discontinuities buried beneath the earth's surface (see e.g. Daniels, 2004). The basic system is composed of a couple of transmit and receive antennas, which are used to propagate wide-band electromagnetic radiation and to detect the backscattering from targets. Arrival time and amplitude of the backscattered radiation are exploited to image dielectric discontinuities. Ursin (1983) proposed a unified treatment of elastic and electromagnetic (EM) wave propagation in horizontally layered media and such formal equivalence allowed sharing procedures for analysis and data processing that are used in exploration seismology. In reflection seismics and GPR, an irregular topography produces variations in traveltime, which are due to the differences in elevation of the source and receiver and need to be corrected, both in single- and multi-fold datasets, with a positive or negative time compensation (static correction) depending on the topography and the position of a reference plane (datum). This is particularly true for GPR data from mound-shaped structures, due to the large topographic gradients. For GPR data there are three different characteristic situations:

(1) the elevation can be considered constant, with flat topographic surface across the offset range;
(2) the elevation cannot be considered constant along the whole GPR profile, but the assumption is valid for each source-receiver pair;
(3) the elevation cannot be considered constant for neither the whole GPR profile and nor for each source-receiver pair.

In the first case no static corrections are required; in the second case a constant correction can be applied for each source-receiver pair, while in the latter case different source and receiver corrections must be applied for each trace. The choice of datum elevation can be arbitrary: the simplest solution is a datum plane located just below the minimum elevation within the profile. Time delay due to the difference in elevation between source and datum is given by:

$$T_t = (E_s - E_d)/v$$

Time delay due to the difference in elevation between a receiving antenna and datum is given by:

$$T_r = (E_r - E_d)/v$$

Total static correction due to elevation is therefore:

$$T = t_s + t_r$$

Correct electromagnetic velocity determination is a crucial task to calculate the time shift for static corrections. Several methods can be applied on such purpose including semblance and constant velocity stack (CVS) analyses on multi-fold data, diffraction hyperbola examination (feasible also on single-fold data), tomographic or vertical radar profiling experiments and migration velocity analyses (Pipan et al., 2001; Hammon et al., 2002; Pipan et al., 2003a,b; Sava et al., 2005; Zhou et al., 2005).

If the GPR survey is performed on a complex topographic surface, methods like topographic migration (Lehmann and Green, 2000) can provide a direct and more appropriate solution, because topography affects wave propagation and static corrections can only partially overcome this problem. As an alternative strategy, common mid point (CMP) gathers can be acquired along straight segments at fix elevation. In such a way no static correction is needed and the velocities required to calculate the time shifts for static corrections can be obtained from moveout analysis.

2.3. Field test

We tested the STG method on a preserved late Bronze Age burial mound in northern Italy (Cassola Guida and Corazza, 2002). The *tumulus* is located in the municipality of Udine, in an alluvial plain. It has a frustum of conical shape with a maximum elevation of about 4.5 m above the surrounding ground level. The average diameter is 26.5 m and the base area is about 550 m^2. We first performed a complete topographic survey with a total station, which resulted in a dataset of several hundreds XYZ points, with precision in the range of ±1 cm.

Fig. 2 shows the location map of the test area (A), a picture of the *tumulus* before excavation (B) and the digital terrain model (DTM) obtained using the measured topographic reference points (C).

2.4. Data acquisition

We completed 12 GPR radial profiles with angular separation of about 15°, all crossing the top of the *tumulus* (Fig. 3). The Ramac system (Malå Geoscience), equipped with 250 MHz shielded and 100 MHz unshielded antennas transmitted a voltage of about 1000 V. Trace spacing was 5 cm and each trace was vertically stacked 64 times in the field to achieve a preliminary reduction of incoherent noise. The sampling

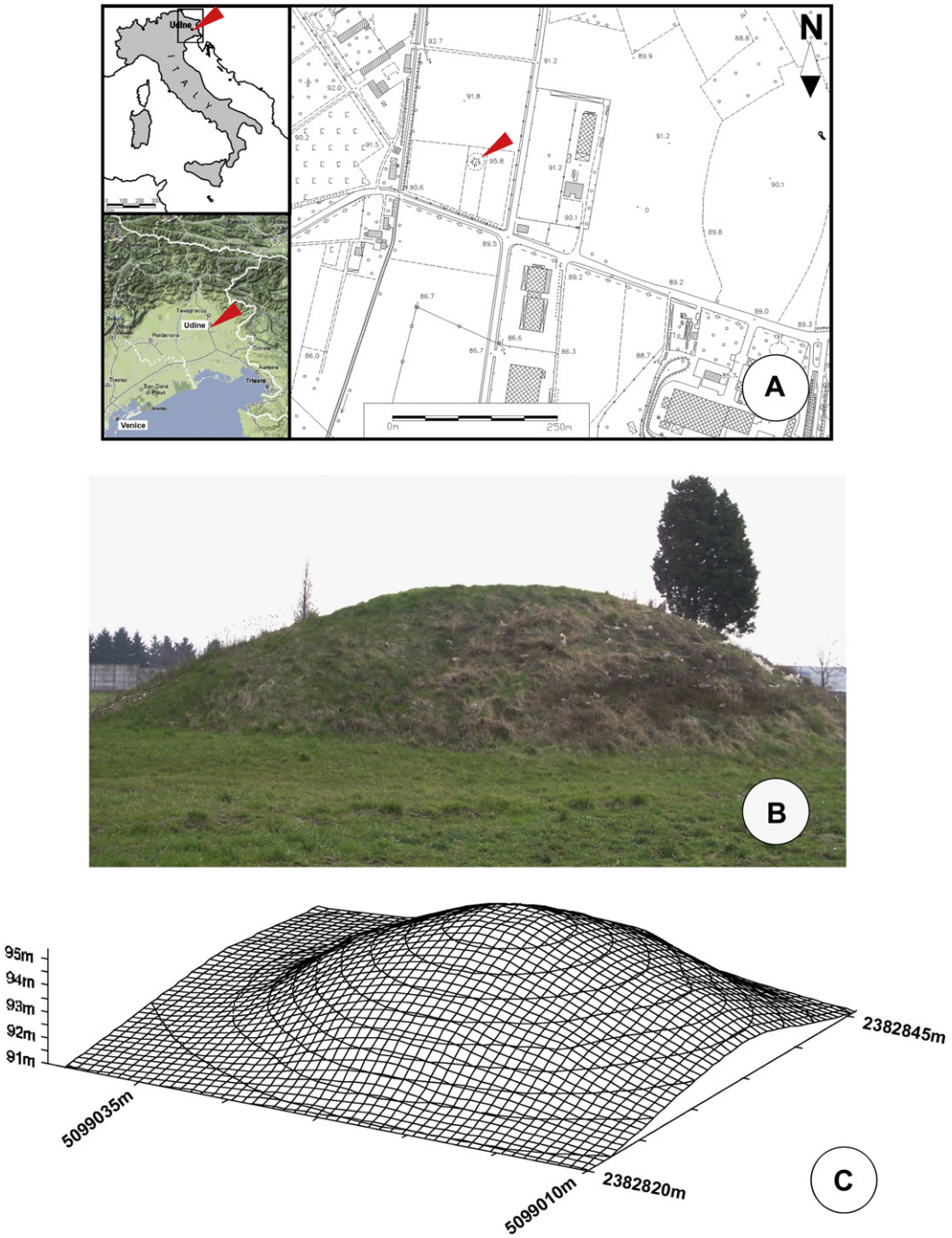

Fig. 2. (A) Location map of the study area; (B) picture of the *tumulus* before archaeological excavation; (C) digital terrain model (DTM) obtained from control points measured with a total station.

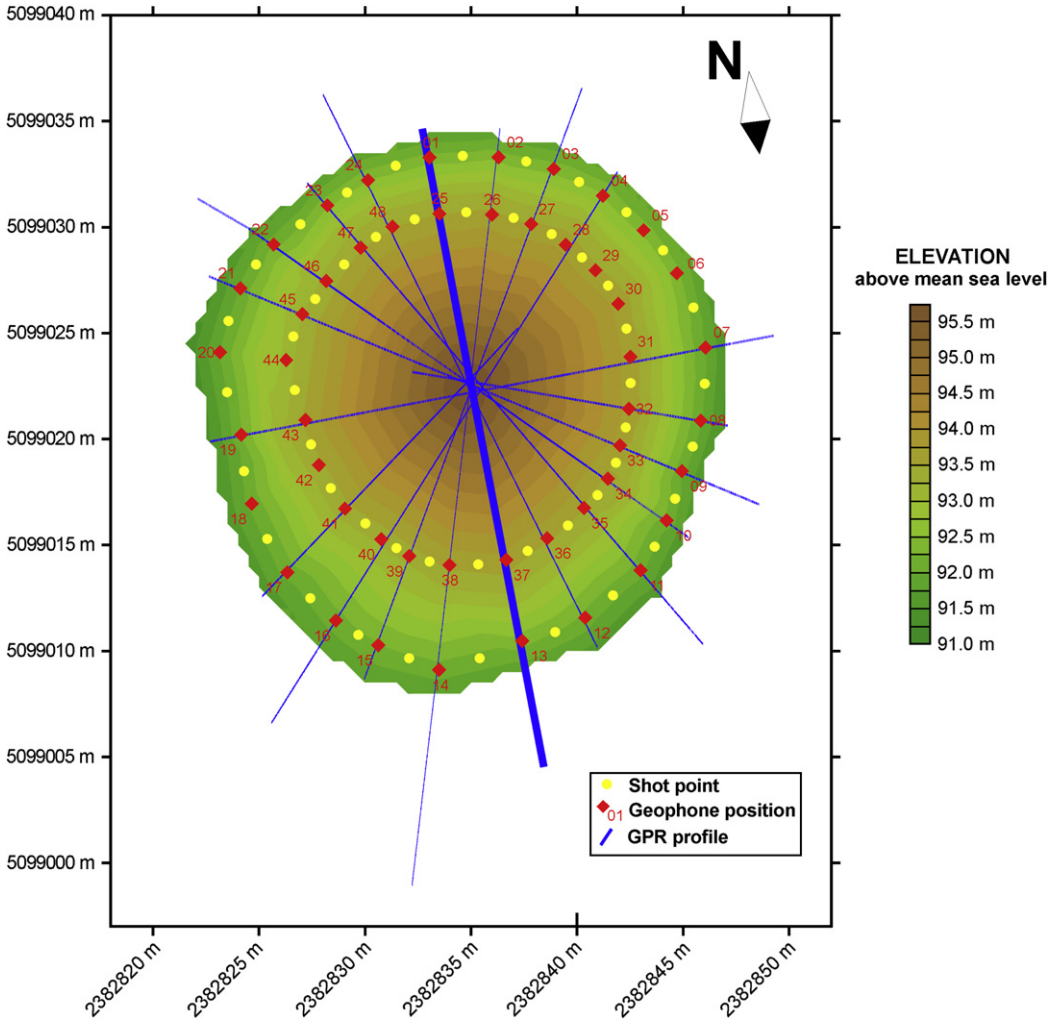

Fig. 3. Color coded elevation map of the tumulus with GPR profiles (in blue), geophone positions (red squares), source positions (yellow dots). The thicker blue line highlights the GPR profile shown in Fig. 4. (For interpretation of the references to colour in this figure legend, the reader is referred to the web version of this article).

rates were 0.4 ns and 0.9 ns with a trace length of 120 ns and 200 ns, respectively. Half-wave dipole transmitter and receiver were oriented parallel to each other and perpendicular to the profile direction to record transverse polarized electromagnetic waves. Radar wave velocity measurements were calculated from 12 common mid point gathers acquired at nearly constant elevation on selected positions of the *tumulus*. We used two 250 MHz shielded antennas in bistatic configuration to perform such measurements. The initial antenna separation was 40 cm with increment steps of 5 cm. The maximum offset was limited to 200 cm to keep transmitter and receiver aligned on straight segments tangent to the surface of the *tumulus*.

For transmission seismic tomography, we used a Geometrics Geode seismograph, 24 vertical geophones with 40 Hz natural frequency and a 2.5 Kg hammer striking a 5 Kg tungsten-chromium steel plate as energy source. The geophones were planted all around the *tumulus* at approximately constant elevation and angular separation of 15° (Fig. 3). Twenty-four source positions between pairs of adjacent geophones were arranged in order to obtain high seismic ray coverage. We performed two seismic tomograms: one at present ground level and one at 1.5 m elevation (geophone positions 01 ÷ 24 and 25 ÷ 48 respectively). We totaled 576 seismic traces for each tomogram.

2.5. Data processing

We applied the following GPR data processing sequence: time zero drift correction, trace editing, background subtraction (i.e. removal of horizontal coherent noise from the radar section to emphasize primary events, see Pipan et al., 2003c, for details), spectral and amplitude analysis, 90 MHz 24 dB/octave–380 MHz 72 dB/octave Butterworth band pass filter, true amplitude correction and predictive deconvolution (Robinson, 1967) with 2.39 ns prediction distance and 31.8 ns operator length. A static correction was also applied to each profile based on detailed topographic measurements. For each trace, source and receiver statics were calculated using an average electromagnetic wave velocity of 10 cm/ns obtained by CMP velocity analysis. The GPR survey exploits a radial data acquisition grid to image shallow features and reconstruct an adequately sampled 3-D subsurface model up to an approximate maximum depth of 3 m. Due to rather high topographic relief and surface gradient (30%, corresponding to a maximum 16.7° dip) a crucial issue in the application of GPR is removal of traveltime deviations due to the irregular data acquisition surface. Lehmann and Green (2000) propose a topographic migration scheme on such purpose, which they show suited to tackle dips greater than 6°. Application of standard processing schemes (i.e. elevation corrections) proves in the present case adequate and

allows reconstruction of dipping events with negligible angular error, as shown by the validation obtained from archaeological excavation. Local velocity variations were detected in the range between 8.9 and 11.2 cm/ns. Tests performed with variable velocities showed negligible improvements in static corrections. Therefore, a constant velocity value was used to correct the topography and to convert sections from time to depth. Complex attributes were eventually calculated and analysed as an aid in the interpretation and in the reconstruction of subtle features in the structure of the mound. We show the results obtained from processing of the 250 MHz data because penetration of EM waves is not actually enhanced in 100 MHz data whilst the resolution level is remarkably lower than in 250 MHz ones. Fig. 4 shows an example of a 250 MHz GPR profile (thicker blue line in Fig. 3) after different processing steps: (A) original profile with an amplitude correction performed with a 23.9 ns wide floating-window automatic gain control (398 ps sampling interval); (B) same profile after static corrections, filtering, true amplitude recovery and deconvolution; and (C) instantaneous phase (i.e. the arctangent of the ratio of the Hilbert transform of the radar trace to the radar trace itself, see e.g. Hardage, 1987) of (B). The fully processed section (Fig. 4B) reveals a complex structure located between 27.5 m and 35 m (horizontal position) approximately. It is characterized by several superimposed levels showing well-defined limits. A V-shaped interruption of the shallow layers, parallel to the topographic surface, shows up at the apex of the mound (marked as v in Fig. 4A,B). A sub-horizontal reflector (*s*) can be traced in Fig. 4A around 4.5 m depth from 0 m reference up to a maximum approximate depth of 2.5 m from topographic surface. The instantaneous phase section (Fig. 4C) allows the identification of horizon (*s*) also in the central

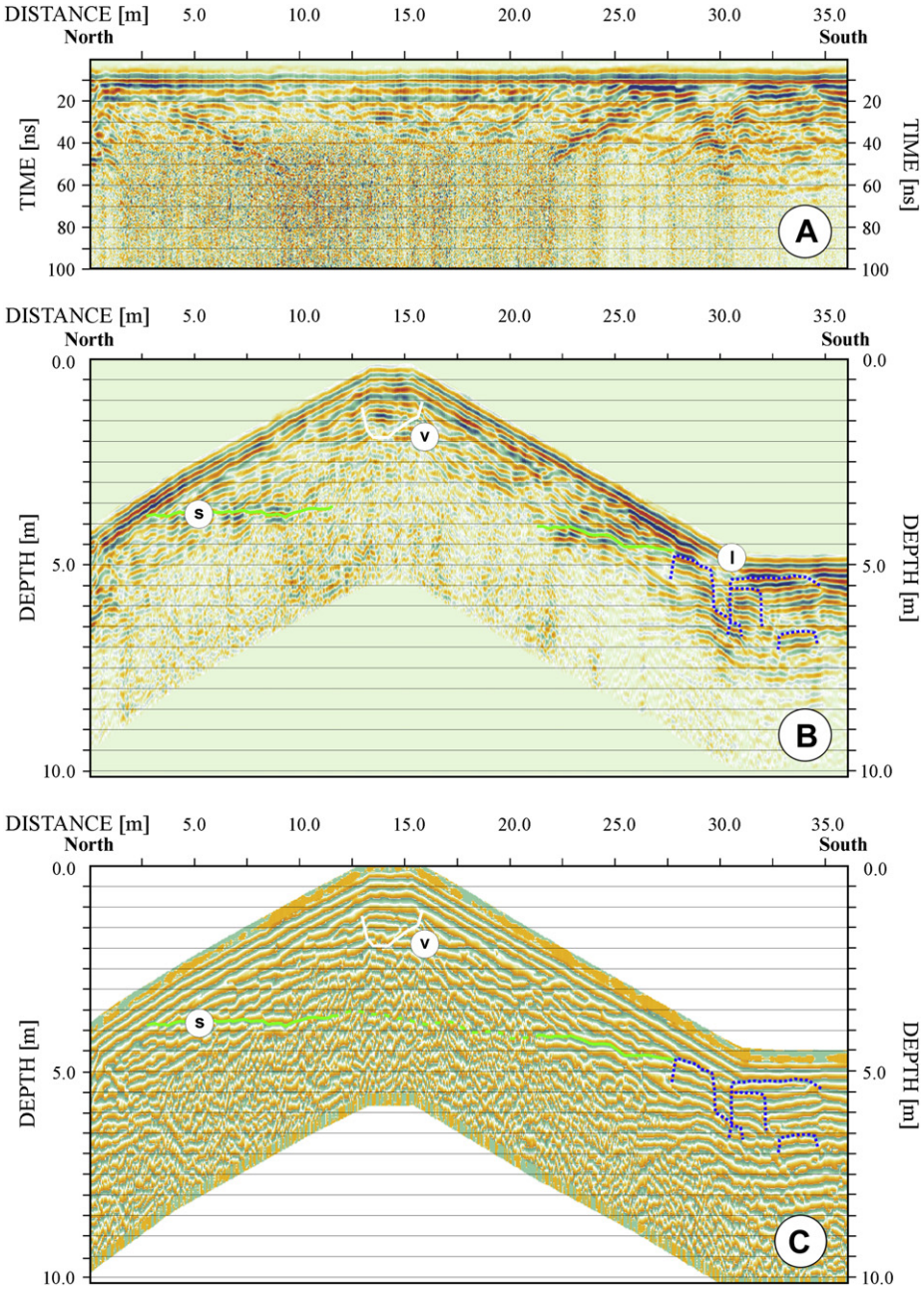

Fig. 4. (A) 250 MHz GPR section after automatic gain control (see Fig. 3 for location); (B) same section after static corrections, filtering, true amplitude recovery and deconvolution; (C) instantaneous phase of profile (B). Vertical exaggeration 2×. (*l*) Lateral structures; (*v*) ancient looting attempt; (*s*) top of silty brown soil. See text for more details.

part of the *tumulus*. The lateral (*l*) reflectors exhibit an irregular pattern, characterized by sub-vertical discontinuities, which differs from the smooth reflectors in the central part of the mound.

As for seismic data inversion, traveltimes were picked from first breaks using an interactive correlation picker that detects zero crossing points and can be optimized for noisy traces. We thus achieved a 100% success rate in first break picking and obtained a high quality 576 traveltimes dataset. We selected 398 raypaths and discharged those related to minimum offset source-receiver pairs because they cross only a pellicular portion of the *tumulus* and provide no useful information for traveltime inversion. We calculated an average velocity of 600 m/s by assuming straight raypaths. The combination of a light (2.5 Kg) hammer with a small and hard plate (ca. 12 cm in diameter, tungsten-chromium steel) produced a quite large frequency band and allowed the design of a computational grid for traveltime inversion based on 400 square cells (1.2 m size). The total number of cells matches the number of rays and the selected cell dimension is based on the $\max\{\Delta x, \Delta y\} = 0.5\, l_{\min}$ criterion (see e.g. Martins et al., 2007). The selected cell dimension can be considered adequate to perform the localization of the burial chamber, which is the primary objective of the study, whilst neglecting details of the inner structure that are beyond the resolving power of the seismic radiation employed.

Minimum and maximum velocities were bounded at 200 m/s (a sub-sonic velocity typical of aerated sediments with low compaction) and 1500 m/s respectively. Positions of receivers and sources were measured with ± 1 centimeter precision in the three coordinates.

We applied SIRT (simultaneous iterative reconstruction technique; Menke, 1984; McMechan et al., 1987; Chen et al., 1990; Brzostowski and McMechan, 1992) to reconstruct the velocity field. We forward modeled curved rays to cope with velocity variations across the *tumulus* due to the high heterogeneity of materials. We adopted the typical flowchart to solve the tomographic problem, i.e. picking of arrival times, 2-D ray tracing through an estimated velocity model, segmentation of raypaths into the pixels of the model, computation of the time residual for each ray, and iterative back projection of the time estimates to produce model updates (Berryman, 1991; Brzostowski and McMechan, 1992).

We discretized the model function in square cells of constant dimension (120 cm $\times$ 120 cm), a solution compatible with the wavelengths involved, which provided an adequate definition of target anomalies (funeral chamber) while exploiting an optimum trade-off as for number of model variables and computational efficiency (Kissling et al., 2001).

The inversion process was iterated several times, by performing cycles of forward traveltime computation, residuals determination, velocity field upgrading. We fixed a convergence limit for a global RMS residual less than 3%. We obtained a RMS residual of 1.02% after seven iterations for the tomogram at ground level (Fig. 5). This value corresponds to a global RMS residual of 0.38 ms, which is comparable with the precision in picking of first breaks. Fig. 5 shows that observed and calculated traveltimes are very similar and the maximum error is limited to an absolute value of 3.26 ms.

Fig. 6 shows the calculated raypaths (in A) and the velocity model obtained after seven iterations for the tomogram at ground level (in B). The orange path highlights an example of bended seismic wave trajectory across the *tumulus*. The raypath analysis shows that the coverage is adequate with negligible shadow zones. The velocity field ranges between 250 m/s in the shallow layer and about 1000 m/s in the inner part of the mound.

We performed tests of dynamic inversion (i.e. amplitude tomography) to gain better insight into subsurface anelastic properties but we obtained a slow convergence on rather high RMS residuals, possibly due to the high sensitivity to errors in picking the first cycle amplitudes.

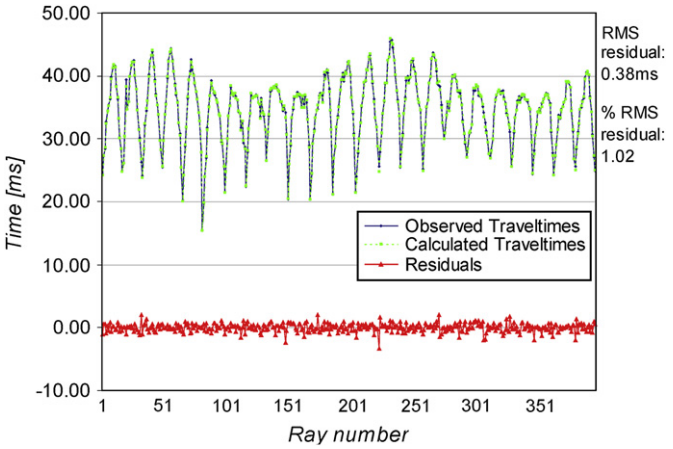

Fig. 5. Observed, calculated and residual traveltimes after seven iterations of tomographic inversion. The complete angular coverage allows a rapid convergence on a final model characterized by small residual error.

2.6. Data integration and interpretation

We integrated all the available processed data to obtain a realistic 3-D interpretation of the *tumulus*. That could be checked with observations and findings of the successive archaeological excavation.

Four main targets can be interpreted in the GPR depth converted radial sections (Fig. 7):

(1) A shallow feature just beneath the apex of the *tumulus* (*v*) with irregular V-shape and a maximum depth of about 1.8 m (Figs. 4B and 7A). The material filling the concave part above the (*v*) reflector shows more attenuation than the surrounding one. Archaeological excavation showed that the (*v*) reflector marks the bottom of an ancient clandestine looting attempt that did not reach the funeral chamber.
(2) Horizons sub-parallel to the *tumulus* flanks (h in Figs. 4B and 7A). They are not regular and show gaps and lenses. Archaeological excavation showed that such levels are correlated with layers of different grain size that were alternated to cover the funeral chamber, in compliance with the peculiar construction method of burial mounds (see e.g. Renfrew and Bahn, 2000).
(3) A sub-horizontal deep reflector (*s* in Figs. 4B and 7A) that cannot be identified in the central inner sector of the *tumulus* because of the radar wave attenuation. Such high amplitude reflector was correlated with the silty brownish material covering the funeral chamber.
(4) Lateral complex structures [(*l*) in Fig. 4B] in the north–eastern and southern sectors of the *tumulus*. The archaeologists found two roman furnaces that exploited the steep flanks of the mound as vertical support and were used to cook limestone. The furnaces were built with irregular stone blocks. Several levels with burnt materials were identified and well correlated with geophysical horizons (Cassola Guida and Corazza, 2002).

The burial chamber cannot be detected from GPR data analysis due to the radar wave attenuation produced by fine-grained sediments (basically silty loams). The enhancement in vertical resolution obtained through deconvolution allowed identifying reflectors less than 20 cm apart. Seismic tomography allows the identification of the velocity anomaly associated with the burial chamber at ground level.

Fig. 8 shows the integrated seismic tomography and GPR (STG) results (A), the burial mound stratigraphy visible after archaeological excavation (B) and the tomb during the skeleton extraction

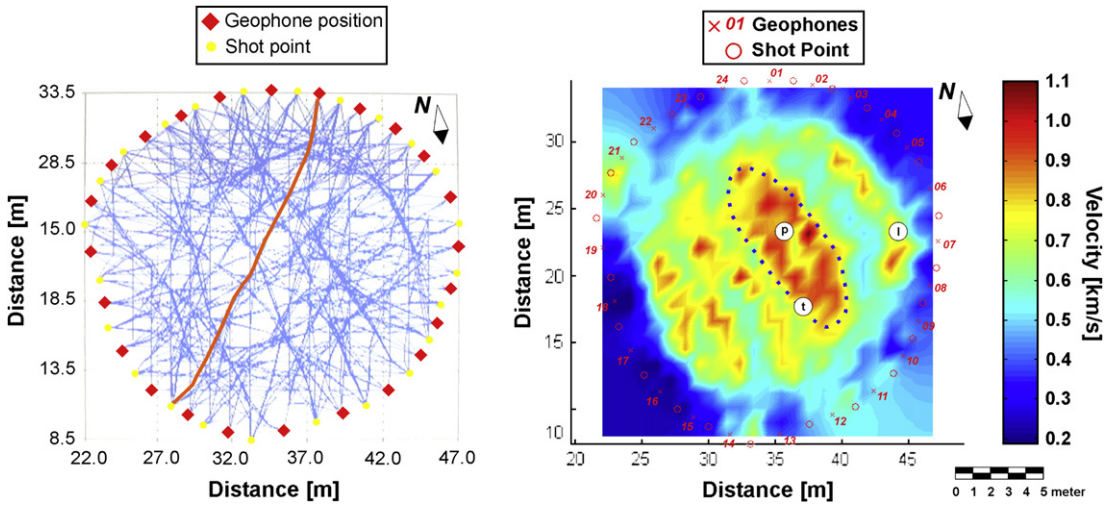

Fig. 6. Seismic tomography: (A) path of seismic rays (in blue) for all source (in yellow) and receiver positions (in red) calculated after seven iteration of inversion process. The orange path shows an example of seismic wave trajectory across the *tumulus*; (B) Velocity map obtained from seismic tomography after seven iterations. (*l*) Lateral structures; (*t*) funeral chamber: perimeter of boulder layer; (*p*) skeleton deposition zone (note that latitude and from longitude coordinates reported in Figs. 2C and 3 are here converted by subtracting constant 5099000 and 2382800 values respectively). (For interpretation of the references to colour in this figure legend, the reader is referred to the webversion of this article)

(C). The high velocity anomaly, close to the central part of the seismic tomogram has elliptical shape with main axis oriented in NNW–SSE direction and can be clearly correlated with the boulders covering the tomb [(*t*) in Figs. 6 and 8A]. Velocity contrast and gradient are high. Dimensions of the velocity anomaly are about 11 m and 5 m in NW–SE and NE–SW direction respectively (Fig. 6B). Such dimensions perfectly match the results of the archaeological excavation. A relatively low velocity zone (*p*) within the anomaly (*t*) could be interpreted as the effect of the skeleton deposition zone, but the cell versus target dimensions ratio does not allow the reconstruction of finer details in the subsurface structure. Localized high velocity anomalies close to the eastern border of the *tumulus* are well correlated with the two roman furnaces discovered by archaeological excavation (Cassola Guida and Corazza, 2002). The traveltime anomaly affects seismic wave propagation at ground level, while is not detected in the tomographic data at 1.5 m elevation.

3. Conclusions

We implemented and tested an integrated seismic tomography and GPR technique (STG) to image the subsurface structure of burial mounds. The method can be applied to mounds of different dimensions, virtually without scale constraints, and it can provide the maximum vertical and horizontal resolution attainable by non-invasive methods on such type of archaeological targets at all depth

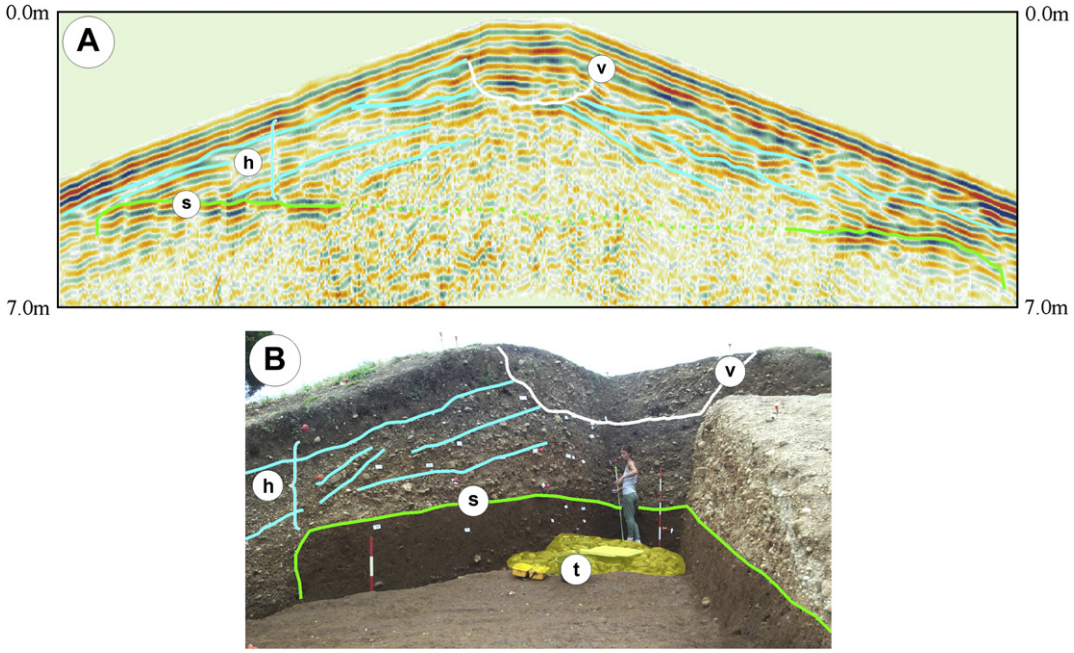

Fig. 7. Comparison between an interpreted depth converted GPR section (A) and results of archaeological excavation (B). (*v*) Ancient looting attempt; (*h*) dipping horizons; (*s*) top of silty brown soil; (*t*) funeral chamber: boulder layer. The inner structure of the tumulus matches the interpreted GPR reflectors within the resolution limits of the radar image and highlights the good correlation between archaeological and geophysical results (see text for details).

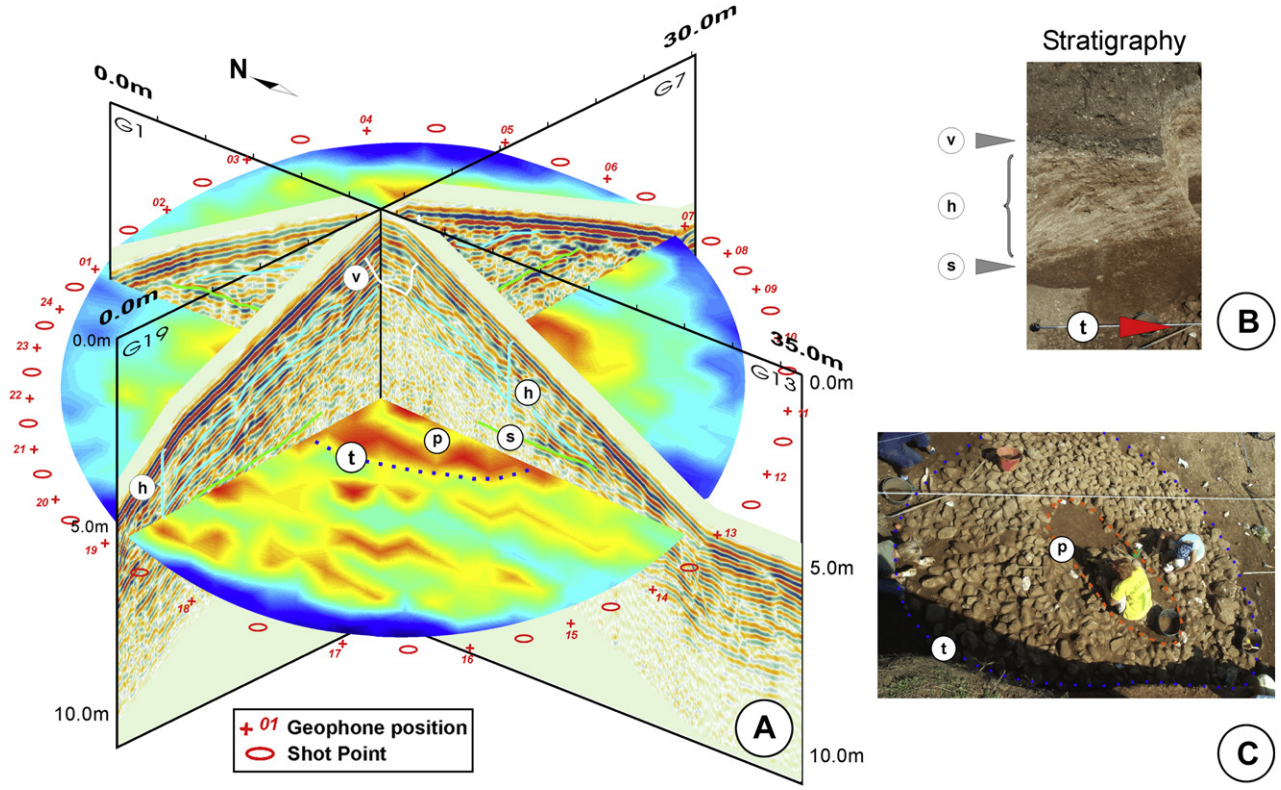

Fig. 8. (A) Geophysical data integration: 3-D view of two GPR sections (G1–G13 and G7–G19) with the seismic tomogram obtained at ground level. (B) *Tumulus* stratigraphy visible after excavation. (C) Detail of the burial chamber after excavation. (*v*) Ancient looting attempt; (*h*) dipping horizons; (*s*) top of silty brown soil; (*t*) burial chamber: boulder layer; (*p*) skeleton deposition zone.

levels by applying adequate sampling intervals to the GPR and tomographic surveys. GPR gives detailed information about the shallow stratigraphy with an approximate resolution of 20 cm, but fails to image the inner part of the structure due to the attenuation of radar waves. In general, penetration of radar waves into burial mounds depends on percentage of clay and use of cobbles/boulders in the construction. The former material is responsible for higher attenuation, the latter for strong scattering. The combination of both phenomena (attenuation, scattering) frequently occurs in *tumuli* because finer and coarser materials were commonly alternated in layers and lenses during construction. The maximum penetration attained in the present case is around 250 cm due to large fractions of clay rich sediments in the shallow part of the mound. Our field experiment demonstrates that GPR can properly image the shallow structure of a *tumulus* with particular reference to layering and construction details. In the proposed case study, features related to successive excavations (looting attempts) or use of the burial mound for different purposes (e.g. furnaces) could also be imaged with GPR data.

The burial chamber is normally located out of reach of electromagnetic waves. Its identification therefore requires complementary techniques. Traveltime transmission tomography is an effective solution on such purpose. In the present case, transmission tomography performed at ground level shows that the burial chamber is characterized by a strong traveltime anomaly. The traveltime anomaly disappears in the tomographic section at 1.5 m, which is above the silty layer covering the funeral chamber (horizon 's' in GPR sections, see Fig. 4B). The large velocity contrast can be considered typical of burial mounds: high velocity materials, such as stone or compacted sediments, normally cover burial chambers. The load of the burial mound may produce a collapse of the burial chamber, which is thus filled by the high velocity materials, as in the present case. Unpublished results from other *tumuli* in NE Italy clearly show the high velocity anomaly even if it is not possible to assess from seismic tomography the conditions of the burial chamber (i.e. collapsed/not collapsed). The archaeological excavation at the study site was based on the information obtained from integrated GPR and seismic tomography. The results confirmed the following qualitative and quantitative indications emerged from geophysical data interpretation: (a) qualitative results: presence and location of targets of interest, general structural scheme of the mound; (b) quantitative results: precise location of targets (x, y, z), depth and dip of layers and lenses, approximate 3-D model of structure and velocity (V–Z). The degree of approximation depends on the adopted spatial sampling: the sampling intervals used in the present case (15° angular separation between GPR profiles, 15° between sensors/sources in the tomographic survey) provided an image of the subsurface structure adequate to plan and successfully complete the archaeological excavation.

The peculiar shape of the target and the possibility of enclosing the mound with sensors and sources deployed in 3-D allows the application of tomographic data acquisition schemes similar to those adopted in computerized axial tomography. In particular, a complete angular coverage of the target can be effectively achieved, which greatly improves the results of tomographic analysis and the identification of anomalies of archaeological interest. Extending the seismic frequency spectrum towards higher frequency can further enhance resolution but is a challenging task in the specific case of the selected study site due to the attenuation of high frequency components by the soft sediments of the mound.

Static corrections are a crucial step in GPR applications to the study of burial mounds. In the present case, the limited depth range allowed to neglect variable velocities in their computation and traditional static computation schemes proved effective, as demonstrated by the successive validation of targets by means of archaeological excavation. Wave equation based methods (see e.g.

Lehmann and Green, 2000) can nonetheless be more appropriate in more complex cases. Dynamic inversion (i.e. amplitude tomography) may provide further information about characteristics of materials and inner structure but it failed to provide useful results in the present case due to high sensitivity of the method to amplitude picking, i.e. minor variations in the choice of the amplitude value of each trace result in substantial differences in the inversion process and in the final model.

In synthesis, the proposed technique may successfully overcome the limitations of the individual GPR and seismic tomography methods by exploiting the benefits of both techniques in terms of penetration and resolution. Moreover, the method can be applied at different stages of the archaeological excavation (while removal of shallow layers is in progress) thus exploiting the superior resolution of GPR at progressively increasing depth within the *tumulus*. We developed a general scheme that can be adapted to structure dimensions, elevation, building materials, characteristics of targets of archaeological interest and logistic constraints.

Acknowledgments

This research was supported by a Halliburton-Landmark academic award, by PRIN-COFIN 2006047924_003, by an Italian Ministry of Foreign Affairs' grant in the framework of bilateral Algerian–Italian cooperation protocol. We are grateful to Prof. Paola Cassola Guida and Dr. Susi Corazza who suggested the field test site and coordinated the archaeological excavation, to Dr. Marco Carnelli for the help during data acquisition and processing and to Dr. Elena Barinova for assistance with archaeological literature. We wish to thank the three anonymous reviewers for their helpful and constructive suggestions.

References

Becker, H., Fassbinder, J.W.E., 2001. Magnetic Prospecting in Archaeological Sites, Monuments and Sites VI. In: ICOMOS (Ed.). Publ. by Lipp GmbH, München, ISBN 3-87490-675-2.

Berryman, J.G., 1991. Lecture Notes on Nonlinear Inversion and Tomography: I. Borehole Seismic Tomography. http://sepwww.stanford.edu/sep/berryman/NOTES/lecture_notes.html.

Bevan, B.W., 1983. Electromagnetics for mapping buried earth features. Journal of Field Archaeology 10, 47–54.

Brooke, A.B., Maillol, J.M., 2007. Multi-offset ground penetrating radar data for improved imaging in areas of lateral complexity — application at a Native American site. Journal of Applied Geophysics 62 (2), 167–177.

Brzostowski, M.A., McMechan, G.A., 1992. 3-D tomographic imaging of near-surface seismic velocity and attenuation. Geophysics 57 (3), 396–403.

Cassola Guida, P., Corazza, G., 2002. Udine, S. Osvaldo tumulo protostorico. Scavi 2002, Aquileia Nostra LXXIII, 754–757 (in Italian).

Chen, S.T., Zimmerman, L.J., Tugnait, J.K., 1990. Subsurface imaging using reversed vertical seismic profiling and crosshole tomographic methods. Geophysics 55 (11), 1478–1487.

Cox, M.J.G., 1999. Static corrections for seismic reflection surveys. Society of Exploration Geophysicists, ISBN 1 56080 080 1.

Dalan, R.A., 1991. Defining archaeological features with electromagnetic surveys at the Cahokia Mounds State Historic Site. Geophysics 56 (8), 1280–1287.

Daniels, D.J. (Ed.), 2004. Ground Penetrating Radar, second ed. The Institution of Electrical Engineers, ISBN 0 86341 360 9.

Fassbinder, J.W.E., Stanjek, H., Vali, H., 1990. Occurrence of magnetic bacteria in soil. Nature 343, 161–163.

Fröhlich Gugler, A.I.M., Gex, P., 1996. Electromagnetic survey of a Celtic tumulus. Journal of Applied Geophysics 35, 15–25.

Hammon III, W.S., Zeng, X., Corbeanu, R.M., McMechan, G.A., 2002. Estimation of the spatial distribution of fluid permeability from surface and tomographic GPR data and core, with a 2-D example from the Ferron Sandstone, Utah. Geophysics 67 (5), 1505–1515.

Hardage, B.A., 1987. Seismic Stratigraphy. Geophysical Press Ltd, ISBN 0-946631-09-3.

Hodder, I., 1984. Burials, houses, women and men in the European Neolithic. In: Miller, D., Tilley, C. (Eds.), Architecture and Order. Basil Blackwell, Oxford.

Kissling, E., Husen, S., Haslinger, F., 2001. Model parameterization in seismic tomography: a choice of consequence for the solution quality. Physics of the Earth and Planetary Interior 123, 89–101.

Le Borgne, E., 1960. Influence du feu sur le propriétés magnétiques du sol et sur celles du schiste et du granite. Annales de Geophysique 16, 159–195.

Lehmann, F., Green, A.G., 2000. Topographic migration of georadar data: implications for acquisition and processing. Geophysics 65 (3), 836–848.

Louis, I.F., 2001. Prospecting for cavities by seismic tomography techniques: the case of Akrotiri Archaeological site. SEG Expanded Abstracts 20, 678–681.

Martins, J.L., Soares, J.A., da Silva, J.C., 2007. Ultrasonic travel-time tomography in core plugs. Journal of Geophysics and Engineering 4, 117–127, doi:10.1088/1742-2132/4/2/001.

McMechan, G.A., Harris, J.M., Anderson, L.M., 1987. Crosshole tomography for strongly variable media with applications to scale model data. Bulletin of the Seismological Society of America 77, 1945–1960.

Menke, W., 1984. The resolving power of cross-borehole tomography. Geophysical Research Letters 11, 105–108.

Monier-Williams, M.E., Greenhouse, J.P., Mendes, J.M., Ellert, N., 1990. Terrain conductivity mapping with topographic corrections at three waste disposals sites in Brasil. In: Ward, S.H. (Ed.), Geotechnical and Environmental Geophysics. Environmental and Groundwater, Soc. of Explor. Geophys., Vol. 2, pp. 41–55. Tulsa, OK.

Morariu, V.V., Bratu, C., Frangopol, P.T., Raileanu, C., 1989. Magnetic prospection of a large tumulus. In: Maniatis, Y. (Ed.), Archaeometry, Proc. 25th Int. Symp. Elsevier Science Publ., pp. 419–425.

Pérez Gracia, V., Canas, J.A., Pujades, L.G., Clapés, J., Caselles, O., García, F., Osorio, R., 2000. GPR survey to confirm the location of ancient structures under the Valencian Cathedral (Spain). Journal of Applied Geophysics 43 (2-4), 167–174.

Persson, K., Olofsson, B., 2004. Inside a mound: applied geophysics in archaeological prospecting at the Kings' Mounds, Gamla Uppsala, Sweden. Journal of Archaeological Science 31 (5), 551–562.

Pipan, M., Baradello, L., Forte, E., Finetti, I., 2001. Ground penetrating radar study of Iron Age tombs in southeastern Kazakhstan. Archaeology Prospection 8, 141–155.

Pipan, M., Forte, E., Dal Moro, G., Sugan, M., Finetti, I., 2003a. Multifold ground-penetrating radar and resistivity to study the stratigraphy of shallow unconsolidated sediments. The Leading Edge 22, 876–881.

Pipan, M., Forte, E., Dal Moro, G., Sugan, M., Gabrielli, P., Finetti, I., 2003b. Interpretive Migration Velocity Analysis with Applications to GPR, Extended Abstracts of EAGE-SEG Research Workshop, Trieste, Italy, 31 August–4 September 2003.

Pipan, M., Forte, E., Guangyou, F., Finetti, I., 2003c. High resolution GPR imaging and joint characterization in limestone. Near Surface Geophysics 1, 39–55.

Polymenakos, L., Papamarinopoulos, S., Liossis, A., Koukouli-Chryssanthaki, C., 2004. Investigation of a monumental Macedonian tumulus by three-dimensional seismic tomography. Archaeology Prospection 11, 145–158.

Renfrew, C., Bahn, P., 2000. Archaeology: Theories, Methods, and Practice, third ed. Thames & Hudson, ISBN 978-0500281475.

Robinson, E.A., 1967. Predictive decomposition of time series with application to seismic exploration. Geophysics 32, 418–484.

Sava, P.C., Biondi, B., Etgen, J., 2005. Wave-equation migration velocity analysis by focusing diffractions and reflections. Geophysics 70 (3), U19–U27.

Tien-when, L., Inderwiesen, P., 1994. Fundamentals of Seismic Tomography. Society of Exploration Geophysicists, ISBN 1 56080 028 3.

Tsokas, G.N., Papazachos, C.B., Vafidis, A., Loukoyiannakis, M.Z., Vargemezis, G., Tzimeas, K., 1995. The detection of monumental tombs buried in *tumuli* by seismic refraction. Geophysics 60 (6), 1735–1742.

Ursin, B., 1983. Review of elastic and electromagnetic wave propagation in horizontally layered. Geophysics 48 (8), 1063–1081.

von der Osten-Woldenburg, H., Chaume, B., Reinhard, W., 2002. Magnetic imaging of a late Bronze Age tumulus in France before and during excavation. The Leading Edge 21, 465–466.

Whiting, B.M., McFarland, D.P., Hackenberger, S., 2001. Three-dimensional GPR study of a prehistoric site in Barbados, West Indies. Journal of Applied Geophysics 47 (3-4), 217–226.

Worthington, M., 1984. An introduction to geophysical tomography. First Break 2 (11), 20–26.

Xu, C.R., Stewart, R.R., 2002. Seismic tomography of Maya pyramid ruins: Belize, Central America. SEG Expanded Abstracts 21, 866–869.

Zhou, H., Sato, M., Liu, H., 2005. Migration velocity analysis and prestack migration of common-transmitter GPR data. IEEE Transaction on Geoscience and Remote Sensing 43 (1), 86–91.